

AIAA-2001-0531

**Direct Calculation of Turbomachinery Flows
Using the Space-Time Conservation Element
and Solution Element Method**

Hsin-Hua Tsuei and Biing-Horng Liou

Concepts NREC

White River Junction, VT

and

S. T. John Yu

Dept. of Mechanical Engineering

Wayne State University

Detroit, MI

DIRECT CALCULATION OF TURBOMACHINERY FLOWS USING THE SPACE-TIME CONSERVATION ELEMENT AND SOLUTION ELEMENT METHOD

Hsin-Hua Tsuei¹ and Biing-Horng Liou²

Concepts NREC

White River Junction, VT

And

S. T. John Yu³

Dept. of Mechanical Engineering

Wayne State University

Detroit, MI

ABSTRACT

Computation of flows in turbomachinery blade rows is critical to aircraft engine design optimization. Traditional Computational Fluid Dynamics (CFD) techniques require an assumption of steady or unsteady flow when these flows are known to include both steady and unsteady effects. The space-time Conservation Element and Solution Element (CE/SE) method is a breakthrough CFD technique, allowing the treatment of steady and unsteady problems with the same calculation. Developed originally at NASA Glenn Research Center, this technique has never before been applied to turbomachinery. The current research applies and validates this new technique for turbomachinery for the first time.

A three-dimensional CE/SE code in cylindrical coordinates has been developed. For the present study, the blade-to-blade flow field was first investigated to address the fundamental issues associated with rotation, and blade-to-blade loading. The algebraic Baldwin-Lomax turbulence model was also implemented to address the shock wave-boundary layer interaction phenomenon. This also marked the first time a traditional turbulence model has been user together with the CE/SE scheme.

A series of validation cases for the newly developed CE/SE scheme for turbomachinery has been conducted. Test cases include the blade-to-blade cross sections of a high pressure ratio, single-stage axial compressor for a commercial small gas turbine engine, NASA Rotor 37, and a single-stage high pressure ratio turbine with a teardrop shaped choked stator. Future developments include extending the CE/SE scheme to full three-dimensional turbomachinery flow calculations,

especially in blade row interaction predictions in multi-stage turbomachines, and secondary flow such as leakage path and seal calculations.

INTRODUCTION

Computational Fluid Dynamics (CFD) for aircraft engine and other turbomachinery design is now commonplace. To be effective for analyzing and designing turbomachinery, practical CFD calculations require the capacity to predict the effects of various complex steady and unsteady flow phenomena like boundary layer formation and growth, flow separation and reattachment, shock wave propagation and reflection, flow oscillations, etc. It is desirable for these CFD models to include multiple blade rows and to model accurately the interaction between the blade rows and the propagation forward and backward through the model of the effects of multiple blade rows, as occurs in the actual flow physics. Many CFD algorithms have been developed and are under continuous refinement, but the need for a new CFD paradigm applicable to wide classes of aerodynamic and aerothermodynamic flow problems has been well established. Current techniques fall short in the gross approximations they require to model the blade row interaction and in the need to separate spatial and temporal effects to different parts of the solution. Traditional CFD methods postulate a steady or unsteady flow field before the calculation is initiated, then based on the steady or unsteady flow assumption, treat the space and time fluxes separately. As a result, a predefined steady-state calculation cannot perform for a physically unsteady problem, and a presumed unsteady calculation proved to be a waste of computational resource for a physically stable flow field.

¹ Head of CFD Section/Corporate Fellow. AIAA Member.

² CFD Engineer. AIAA Member.

³ Associate Professor. AIAA Member.

Although there is the need to calculate more accurately all of the complex flow physics in turbomachinery, of particular interest in turbomachinery flow applications is the prediction of rotor-stator interactions in multistage axial gas turbines. The understanding that has been developed to date, regarding the rotor-stator interaction phenomenon, has led to many new design concepts, for both compressors and turbines, to take into account in the engine design the interactions between blade rows. Nevertheless, this job has been made more difficult because analytical techniques for predicting these complex interactions have lagged the growing needs for better understanding of these effects on the turbomachinery stability and performance. One of the reasons why development of sufficiently effective analytical techniques has been difficult is that blade row interaction in turbomachinery includes both steady and unsteady effects and it has not been possible to treat steady and unsteady effects together in the same solution. The proposed analytical method represents a breakthrough in CFD techniques in that it allows, for the first time, the ability to treat steady and unsteady problems with the same calculation. Developed originally at NASA John Glenn Research Center (GRC), this technique has never before been applied to turbomachinery. This innovative STTR program proposes to apply this new technique to turbomachinery for the first time, offering a step increase in computational accuracy for analysis of turbomachinery.

The design of both compressor and turbine blade rows must account for blade row interaction. For example, in a compressor rotor stage, from the leading edge of the rotor blade, low momentum gas tends to migrate toward the tip section. The migration of the low momentum fluid is a steady blade row interaction phenomenon. If the gap between the rotor and stator is too large, the low momentum gas quickly fills up the tip section, causing degradation in the compressor performance. From this point of view, the gap between the rotor and stator should be kept as small as possible to reach optimum performance. However, because of the unsteady wake generated by the rotor trailing edge, if the gap is too small, the wake will not be well mixed out before it enters the stator blade passage. The unsteady wake-induced blade row interaction exhibits unsteady flow physics. As a result, the pressure and velocity gradients in the wake flow impinging on the stator blade will cause the stator structure to oscillate. From this point of view, the gap between the rotor and stator should be determined on the rotor performance and blade geometry, instead of being based on the low momentum gas migration alone. This is an example of where looking at steady or unsteady physics separately would result in a misleading conclusion. Only when steady and unsteady effects are considered together can the correct design decision be reached.

Wake-induced rotor-stator interaction often impacts the design of a turbine stage as well. A comprehensive review of the impact of unsteady blade row interactions on turbine design concepts and procedures was given by Sharma et al. [1]. The unsteady pressure fluctuation from the wake of the upstream stator can cause the rotor cooling flow to be unable to exit the cooling holes on the rotor surface as expected, impacting the effective cooling of the blade. There are several options available to address this problem. First, the gap between the stator and rotor can be increased to allow enough mixing in the stator wakes to minimize the pressure oscillation effects on the rotor. However, over-compensating the unsteady fluctuation will again reduce the overall turbine stage performance. Second, the cooling hole location, size, and the amount of cooling flow can be redesigned to accommodate the pressure oscillations. The optimum design needs to seek a balancing point in the cooling effects and overall stage performance. However, to achieve this delicate balance, a detailed understanding of these flow physics is required. Accurate computation of blade row interaction is one of the fundamental issues in turbomachinery performance and flow field predictions and is clearly needed. New techniques for accurately calculating steady and unsteady effects in multiple blade rows is an important enabling technology for both aerospace and industrial turbomachinery.

The present work addresses this need through the development and validation of a unique numerical approach that contrasts strongly with traditional CFD algorithms. This new CFD technology, the so-called "Space-Time Conservation Element and Solution Element (CE/SE) Method," or "CE/SE method" for short, was developed by Dr. Sin-Chung Chang [2,3], a Senior Research Scientist at NASA GRC (formerly NASA Lewis Research Center). This technique promises a step increase in accuracy for blade row interaction computations in turbomachinery flows, especially in gas turbines. The proposed space-time CE/SE method is an innovative breakthrough in CFD technology which treats the spatial and temporal fluxes as an integrated union, instead of separating the two by assuming steady or unsteady flows, as is done in traditional CFD schemes. As a result, a steady or unsteady solution obtained using the Space-Time CE/SE method depends entirely on the nature of the flow, not on an assumed steady or unsteady condition. Therefore, time accurate solutions for complicated rotor-stator interactions often encountered in turbomachinery flows, including unsteady wake, dynamic (unsteady) shock reflection, and unsteady shock-tip leakage vortex flow interaction, can be obtained without additional presumptive conditions. Further, the proposed numerical model is specifically intended to be general in nature, so that little or no manual manipulation of the modeling parameters should be required to achieve accurate solutions of flows within broad application areas,

leading to substantial improvements as compared to current CFD technology. For example, it is already proven that greater accuracy can be achieved for “time-accurate” shock wave predictions with the proposed Space-Time CE/SE technique, when compared to existing CFD methods, while no added artificial smoothing is necessary [4,5].

The current study seeks not only to develop this model, but also to validate its effectiveness and accuracy specifically for turbomachinery flows which are, without a doubt, some of the most complex of all flow conditions. When fully developed and validated for these complex turbomachinery flows, it is expected that this advanced CFD scheme will also be applicable to a wide range of other flow conditions. These could include flows around airframes, engine ducting, control surfaces, weapons and separable stores, plus general flows involving such phenomena as rotation, separation, transition, convective heat transfer, skin friction, mixing, and combustion. The benefits of having such an improved CFD algorithm will be more accurate CFD solutions and improved understanding of steady and unsteady blade row interaction effects, leading to reduced engine design cycle time, improved design capabilities, and reduction in the number of physical model tests required to finalize a design. The end results of better understanding of blade row interactions, including how to account for them in the design process, could include greater engine stable operating range, reduced specific fuel consumption, longer engine life, and improved safety. The proposed technology will have broad commercial use in CFD programs for design optimization of aircraft turbine engines, plus a tremendous array of industrial equipment, including industrial compressors, turbochargers, refrigeration compressors, turbopumps, and both steam and gas turbines for power generation and marine applications.

Efforts and CFD Techniques on Rotor-Stator Interaction Flow Field Simulation in Turbomachinery

With the advancement of CFD technology and computer speed, three-dimensional (3D) CFD calculations have become a routine part of the engineering design process, not only for turbomachinery, but for many industrial applications as well, ranging from chemical mixing processes to automobile engines. In turbomachinery flows, full-3D CFD analysis, for a single blade row as well as for multiple coupled blade rows, has greatly enhanced our understanding of these complex flow fields and has enabled significant design improvements. Three-dimensional calculations serve as a numerical laboratory to provide visualization of the complicated turbomachinery flow field. Details of gas turbine flow field phenomena, such as shock-tip leakage vortex interaction and unsteady shock-boundary layer structure through blade row interaction, have been discovered. With the understanding gained from the full-3D CFD

analysis, the turbomachinery design philosophy has again changed over the past several years. Multiple blade row simulation has enabled the understanding of the influence of blade row interaction on global machine performance, as well as local flow field characteristics. With this fact in mind, the impact of a better CFD predictive capability on the overall improvement of the turbomachinery industry is profound.

Turbomachinery flows, especially in gas turbines, include a variety of complex flow phenomena, including laminar-to-turbulent transition and relaminarization, adverse pressure gradients, shock wave and flow discontinuity, flow separation, secondary flow mixing, rotor-stator interaction, tip clearance flows, combustion, and heat transfer. Each of these flow characteristics must be taken into account in turbomachinery engineering. In coupled rotor-stator analysis, all of the above mentioned, except combustion, are present in the flow analysis. In this proposal, we will limit the focus to non-reacting flows. Integrated chemically reactive combustor/turbine flow analysis using the Space-Time CE/SE scheme is definitely of value and might be addressed in the future as a separate technical effort, building on the foundation established by the present work.

For rotor-stator interaction computations, a common thread is the blade row interface treatment. There have been a number of algorithms developed for the blade row interface modeling in rotor-stator interaction calculations. The inter-row mixing plane method [6,7] assumed that the flow is steady, relative to each individual blade row. This model uses a circumferential averaging technique to provide communication between the blade rows. The gradients are smeared out in the circumferential direction, yet preserved in the radial direction. This inter-row mixing plane technique provides a fundamental mechanism to simulate rotor-stator interaction. However, flow information can be lost through the averaging process. Obviously, the unsteady wake-induced rotor-stator interaction and its related issues are not resolved by using this approach.

The average passage technique [8,9], like the proposed CE/SE method was developed at NASA GRC, provides row-by-row solution with sophisticated averaging to represent the “missing” rows in the multiple blade row environment. In this approach, steady 3D equations are solved separately in each blade-to-blade passage in each of the blade rows of a multistage machine. This approach allows a practical steady 3D methodology for multistage turbomachinery computations. Unsteady effects caused by neighboring blade rows are averaged out in time, and information about the neglected unsteady effects is transported from one row to another. The computational domain of a given blade row is expanded to include only the space occupied by the downstream/upstream blade row, however, not the actual blade row

itself. The effect of pressure difference across a blade surface and the resultant flow turning is introduced through steady body-force for the missing blade row, while the unsteady effect is modeled by using 'deterministic' stresses. Some of the modeling parameters have been modified specifically for multistage compressor calculations [10,11].

Unsteady flow analysis using a combined "patched and overlaid" grid method for blade interface has been applied to 2D rotor-stator interaction simulation in an axial turbine [12]. This technique splits up the interface region between blade rows into four zones, then applies appropriate interpolation procedures on these patched or overlaid grids. Computational results indicated unsteady pressure existed in between the 2D turbine stator-rotor blades. The computed time-averaged results compared well with measured data, but the magnitude of the pressure fluctuation did not agree with measured data. This disagreement could be a result of the 2D computational model, which is not appropriate for highly 3D rotor-stator interactions.

A quasi-3D rotor-stator analysis was developed for the first stage of the SSME high-pressure fuel turbopump [13]. In this study, the blade-to-blade plane was analyzed, though the stream surface thickness in the hub-to-tip direction was taken into consideration. The blade row interface was modeled through a line of overlap "dummy cells" to impose periodic or overlap boundary conditions. At this overlap gridline, flux variables in the stator are interpolated to obtain rotor quantities, while flux variables in the rotor are interpolated to acquire stator flow variables. Unsteady computations for a 1:1 and a 2:3 stator-rotor blade ratio were made. The 2:3 blade ratio was close to that of the real machine. The computational results showed that the blade count ratio has an influence on the unsteady characteristics and fluctuation magnitude.

With the steady increase in available computational power, numerous researchers are now conducting CFD calculations for unsteady, 3D, full Navier-Stokes equations for rotor-stator interactions. This has increased the understanding of rotor-stator interaction physics one step further in order to provide a numerical wind tunnel for turbomachinery designs. The effects of rotor-stator interactions were studied, with the help of experimental data, to conduct 3D unsteady CFD calculations for stator and rotor separately for an axial turbine stage [14]. The measured inlet conditions were used to calculate the stator flow field. Vortex shedding from the stator blade trailing edge can be observed. The rotor inlet used measured time-variant data downstream in the stator wake region to proceed the 3D unsteady oscillation. It was found that the wake and secondary flow structure in the rotor blade passage were largely influenced by the unsteady inlet oscillation. The numerical simulation suggested that the secondary flow/blade

interaction might have a dominant effect on unsteady blade loading and noise production.

Investigation of the rotor-stator interaction continued to include the fully-coupled 3D unsteady calculation for rotor-stator configurations. The unsteady aerodynamics of a high through flow transonic compressor stage were studied [15], and the time-averaged computational results were compared with experimental data. The numerical simulation was limited to a calculation of a specified blade count ratio for the rotor and stator blades, with assumed periodicity on the outermost tangential direction, instead of modeling the entire 360° compressor stage. Theoretically speaking, modeling the entire stage is possible, although the computational cost associated with such a calculation is too high by today's standards. To model the interface, the sliding mesh technique was used to provide communication across the blade row interface. The sliding mesh was established by using one overlaid grid line, then 2D interpolation for the flow variables and gradients was performed on this plane to transfer information from rotor to stator, or vice versa. In this study, higher order accurate schemes, both in space and time, have to be utilized to prevent excessive numerical dissipation, and to provide enough resolution across the blade row interface. Computational results revealed a separation region near the stator tip section, resulting from a high incidence angle caused by the rotor tip clearance flow. Because of the unsteady wake, the separation was not found to be periodic for each stator blade passage. A similar study can be found in [16].

Because traditional CFD methods automatically separate the space and time domains, the difficulties encountered in modeling the blade row interface rotor-stator interaction are a subject of ongoing research. Research and development efforts have continued over the past few years to seek better means within the traditional CFD framework to improve the interface modeling in order to enhance solution accuracy. A very comprehensive review of how these traditional CFD techniques, and their limitations when applied to turbomachinery flow predictions, were given in [17]. Details on how each individual technique performed for turbomachinery flows will not be repeated here.

In contrast to these traditional CFD schemes, the blade row interface boundary condition for the CE/SE scheme is surprisingly simple. As the solution marches in the space-time domain, the space-time flux and flow variables are extrapolated into the next time step for both the rotor and stator. Since space and time fluxes are united in the space-time domain, the rotor mesh simply rotates to the next position in both space and time, and the stator mesh stays in the same spatial location, but has a new time frame. For example, for a two-dimensional (2D) rotor-stator mesh, the space-time mesh is 3D, with time

frame being the third dimension. The 3D space-time mesh changes shape at each time step. Therefore, in the space-time domain, the blade row interface simply turns out to be one of the interior solution domains for the CE/SE scheme. As a result, the interface modeling issues raised by conventional CFD schemes because of rotor motion, such as circumferential averaging or sliding mesh and interpolation, do not apply for the CE/SE scheme. The mathematical formulation is given in the theoretical section of this proposal to describe this moving frame concept in CE/SE scheme.

Another additional, and already proven, advantage of the CE/SE method over existing CFD methods is CE/SE method's ability to accurately capture shock waves. Shock capturing techniques are also a subject of ongoing research, not only for turbomachinery flows, but in all types of transonic or supersonic flow field predictions. There have been many claims of improved CFD algorithms which have later disappointed users. The common trend of these CFD schemes is that one or a combination of several artificial damping techniques [18,19] are involved that can mask the real flow physics by smearing out the discontinuity too much in order to provide numerical stability. Past efforts at improved shock wave capturing have historically exhibited poor results because they improved accuracy only for a simplified flow condition, such as a one-dimensional (1D) shock tube. These techniques have often neglected more complicated issues, like shock reflections, shock wave-boundary layer interactions, and the unsteady shock wave-boundary layer structure that results from unsteady rotor-stator interactions in a turbomachinery environment.

The reason traditional shock capturing techniques faltered was that they were developed under the assumption that the 1D Riemann variable is valid for all three directions. Therefore, these techniques all appeared in a 1D form, even though they were used for predicting 3D wave propagation characteristics. Direct applications of 1D based techniques to 3D problems resulted in distorted 3D wave fronts [20]. In gas turbines, due to blade row interaction, the oblique shock near the tip section of a compressor rotor is often influenced by the unsteadiness resulting from the wake of the upstream stator and the unsteady pressure oscillations caused by downstream blade rows. The location of the shock, as a result, will oscillate near the rotor tip. Existing techniques are ill suited to predict this behavior, while the CE/SE technique has been shown to model this behavior well.

The CE/SE method treats space and time simultaneously and has demonstrated accuracy in resolving 3D shock waves. The ability of the CE/SE method to capture 3D shocks while preserving the flow physics is unprecedented. The proposed Space-Time CE/SE method is based on integrated space-time flux (instead of the historically-separated spatial flux terms

plus the temporal flux, if unsteady) using a Solution Element (SE) constructed on the space-time plane. The details of constructing a unified space-time flux on the SE, based on a Conservation Element (CE) of the Space-Time plane, will be given in the following section of this proposal. The proposed CE/SE method was developed to solve multi-dimensional problems and the importance of simplicity and generality weighed heavily in its design. Characteristics-based techniques were avoided to eliminate presumptive conditions for the Navier-Stokes equations.

NUMERICAL FORMULATION

The Space-Time Conservation Element and Solution Element Method, or the CE/SE Method, originally proposed by Chang [2-5], is a new numerical framework for conservation laws. The CE/SE method is not an incremental improvement of a previously existing CFD method, and it differs substantially from other well-established methods. The CE/SE method has many non-traditional features, including a unified treatment of space and time, the introduction of conservation element (CE) and solution element (SE), and a novel shock capturing strategy without using Riemann solvers. To date, numerous highly accurate solutions have been obtained [2-5], including traveling and interacting shocks, acoustic waves, shedding vortices, detonation waves, shock/acoustic waves interaction, shock/vortex interaction, and cavitations. The design principles of the CE/SE method have been extensively illustrated in the cited references. In this paper, a brief description of the CE/SE method is provided as the background of the present work.

Perhaps one of the most important features of the CE/SE method is the adoption of a space-time integral formulation as the cornerstone for the subsequent numerical discretization. Note that one derives the conventional finite-volume methods based on Reynolds' transport theorem, in which space and time are not treated equally. Thus, the space-time geometry of a finite volume is restricted such that classical Riemann problems were encountered in calculating flux conservation. In contrast, due to an equal footing treatment of space and time, Chang's integral formula allows a better choice of space-time geometry of CEs in calculating flux conservation, and the Riemann problem is avoided.

The Reynolds Transport Theorem

The conventional finite-volume methods for simulating the conservation laws were formulated according to flux balance over a *fixed spatial domain*. The conservation laws state that the rate of change of the total amount of a substance contained in a fixed spatial domain V is equal to the flux of that substance across the boundary of V , i.e., $S(V)$. Let the density of the substance

be u and its spatial flux be f , the convection equation can be written as

$$\frac{\partial u}{\partial t} + \bar{\nabla} \cdot \bar{f} = 0 \quad (1)$$

According to the Reynolds transport theorem, the integral form of the above equation can be expressed as:

$$0 = \frac{d}{dt} \int_{V(t)} u dV = \frac{\partial}{\partial t} \int_V u dV + \int_{S(V)} \bar{f} \cdot d\bar{s} \quad (2)$$

The transport equation provides the bridge between the Lagrangian frame the Eulerian frame. The conventional finite-volume methods concentrated on calculating the surface flux, i.e., the last term of Equation (2). The time derivative term of Equation (2) is usually calculated by a finite difference method, e.g., the Runge-Kutta method, or a temporal integration:

$$\int_V u dV \Big|_{t_1}^{t_2} = \int_{t_1}^{t_2} \left(- \int_{S(V)} \bar{f} \cdot d\bar{s} \right) dt \quad (3)$$

Due to the *fixed spatial domain*, the shape of the Space-Time Conservation Elements (CEs) in one spatial dimension for Equation (3) must be rectangular. Refer to Figure 1(a). These elements must stack up exactly on the top of each other in the temporal direction, i.e., no staggering of these elements in time is allowed. For equations in two space dimensions, as depicted in Figure 1(b), a conservation element is a uniform-cross-section cylinder in the space-time domain, and again no staggering in time is allowed.

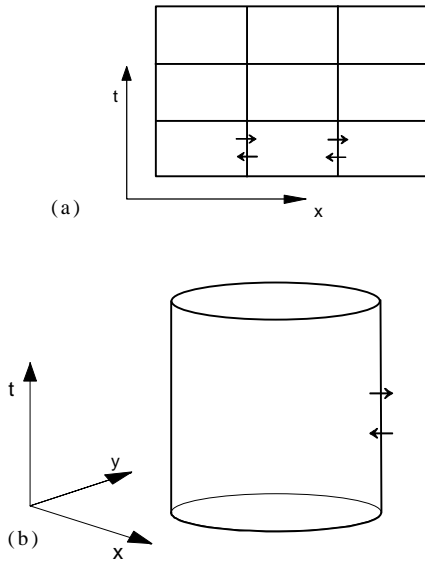


Figure 1. Space-time integration for conventional finite-volume methods.

This arrangement results in vertical interfaces extended in the direction of time evolution between adjacent space-time conservation elements. Across these interfaces, flow information travels in both directions. Therefore, an upwind bias method (or a Riemann solver) must be employed to calculate the interfacial fluxes. The Space-Time Integral Formula

Equation (1) is a divergence free condition, i.e.,

$$\nabla \cdot \bar{h} = 0, \quad (4)$$

where the current density vector $\bar{h} = (f_x, f_y, f_z, u)$. According to the divergence theorem, we have

$$\oint_{S(V)} \bar{h} \cdot d\bar{s} = 0 \quad (5)$$

Figure 2 is a schematic for Equation (5) in one spatial dimension.

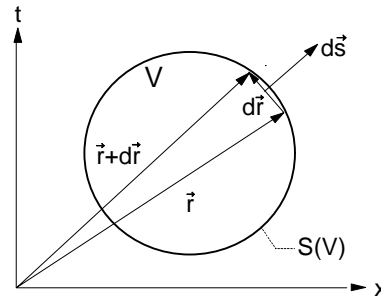


Figure 2. A schematic of the space-time integration [1].

We remark that space and time are treated in an equal footing manner, and there is no restriction on the space-time geometry of the CEs.

The CE/SE Method

Based on the above integral equation for space-time flux balance, Chang proposed a new numerical framework for conservation laws. The CE/SE method is a family of schemes, i.e., the a scheme, the a - e scheme, and the a - a scheme. The a determines the space-time geometry of the numerical mesh employed. The a - e and the a - a schemes are extensions of the a scheme for nonlinear equations and for shock capturing.

First, the space-time domain of interest is divided into many Solution Elements (SEs). In each SE, flow variables are assumed continuous. A first-order Taylor series is used by Chang to discretize the flow variables. Thus the scheme is second-order accurate. Across the boundaries of neighboring SEs, flow discontinuities are allowed. Flow variables are calculated through a local

space-time flux balance, which is enforced by integrating over the surfaces of a Conservation Element (CE). Unlike SEs, various CEs could be imposed for local and global space-time flux balance.

In Chang's a scheme, the number of the CEs employed matches the number of unknowns designated by the scheme. In addition to the flow variables, the spatial gradients of flow variables are also treated as unknowns. As a result, two CEs are used to solve a one-dimensional convection equation, Equation (2.1.4), because the variable u and its spatial derivative u_x are the unknowns. Similarly, three CEs are used for two-dimensional equations, because u , u_x , and u_y are the unknowns, and four CEs are used for the three-dimensional convection equation. As shown by Chang, triangles and tetrahedrons are used as the basic mesh stencil to construct the necessary CEs for two- and three-dimensional equations. We remark that unlike the modern upwind schemes, flow variable distribution inside a SE is not calculated through a reconstruction procedure using its neighboring values at the same time level. Instead, they are calculated as a part of local space-time flux conservation.

In matching the flow solution, the flow variables at neighboring locations leapfrog each other in time in a zigzagging manner. Refer to Figure 2.1.3 for equations in one spatial dimension. This is achieved by imposing the space-time integration over rhombus-shape CEs. In this case, the CEs coalesce with SEs. Through each oblique interface between adjacent CEs, flow information propagates only in one direction, i.e., toward the future. Therefore, no Riemann problem is encountered and the use of a Riemann solver to catch shocks is avoided. The resultant a scheme is non-dissipative (or neutrally stable) for linear waves. One can match the solution from a specific space-time point first forward in time and then backward to recover the initial condition of the flow variables — the a -scheme is space-time inversion [2-5]. As pointed out by Chang, conventional schemes lack space-time inversion due to the inherent artificial damping.

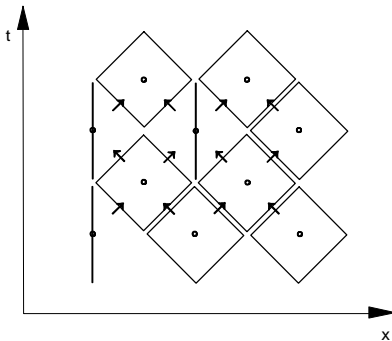


Figure 3. A schematic of the CE/SE method in one spatial dimension.

It is noteworthy that the treatment of the non-reflective boundary condition in the CE/SE method is very simple [2-5]. Usually, one simply extrapolates the flow variables to the mesh point in the staggered position at a future time step. In general, nearly perfect non-reflective boundary condition can be achieved.

When applied to nonlinear equations, e.g., the Euler equations, the above a scheme is modified by adding artificial damping for numerical stability. The result is the a - e scheme. In particular, within one time matching step, only the calculations of u_{mx} , u_{my} , and u_{mz} are impacted, while the calculation of u_m is kept intact as that in the original a scheme. Note that $m = 1, 2, 3, 4$, and 5 for the five equations in the Euler equation set in three spatial dimensions. When contact discontinuities appear in the flow solution, the calculation of u_{mx} , u_{my} , and u_{mz} is further modified by a re-weighting procedure to filter out spurious oscillations. The result is the a - a scheme with a as the weighting parameter. Since the original a scheme is neutrally stable, locally, the calculation of u based on the a scheme is not contaminated by artificial damping and/or the re-weighting procedure. The careful management of the numerical damping by Chang contributes to the high accuracy of the CE/SE method, when the method is only second-order accurate.

However, by adding the artificial damping, the flow variables gradients, calculated by the a - a and a - e schemes, do not satisfy the space-time flux conservation over the original CEs. Thus, the property of space-time inversion and non-dissipation is lost. Therefore, in applying the CE/SE method to nonlinear equations, the calculations of (u_{mx}, u_{my}, u_{mz}) are distinctly different from the calculation of u_m . This deviation in calculating (u_{mx}, u_{my}, u_{mz}) from that in the original a scheme provides a window of opportunity to modify the CE/SE method such that the CEs are specified only for u_m . The algorithm of calculating (u_{mx}, u_{my}, u_{mz}) could be modified based on a usual central differencing scheme. As it will be illustrated in the following sections, this modification allows the flexibility of using general polygons and polyhedrons for two- and three-dimensional flow equations.

The original CE/SE method is modified in the present project such that only one CE at each grid point is employed for equations in one, two and three spatial dimensions. As a contract to the original CE/SE method, the CE in the present method is used only to calculate the flow variables, while the spatial gradients of the flow variables are calculated by a central differencing method. For equations in two spatial dimensions, the present method allows the use of quadrilaterals and/or polygons in either structured or unstructured meshes. For equations in three spatial dimensions, general polyhedrons can be used as CEs. Thus, the present modified CE/SE method is applicable to general unstructured meshes with mixed elements of various shapes. As such, it can serve as an

alternative solver for time-accurate solutions in well-established CFD codes.

In the present method, the flow variable gradients (u_{mx} , u_{my} , u_{mz}) are calculated based on a central difference type reconstruction method, which is similar to Chang's α - ϵ scheme for one-dimensional equations. Because of the finite-difference reconstruction, the present method can be straightforwardly applied to structured mesh for flows in two and three spatial dimensions.

RESULTS

Single-Stage Compressor for a Small Commercial Gas Turbine Engine

To evaluate the CE/SE turbomachinery results compared with traditional CFD schemes, we started by running the solver through a series of test cases. The computed CE/SE results are compared to results obtained from the traditional Runge-Kutta (RK) scheme developed in [6,7], by using identical geometry, grid size and distribution, and machine operating conditions to provide a fair assessment.

The first test case was a one stage transonic compressor. This compressor was developed for a small gas turbine engine for business jets (Yoshinaka, T. and LeBlanc, A. D., 1981).

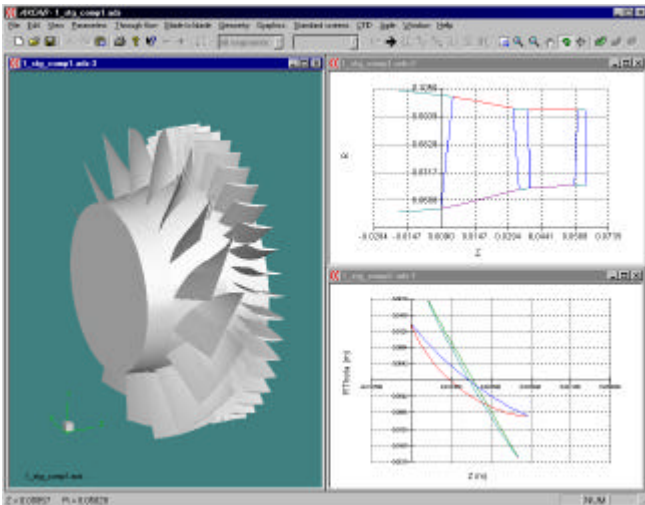


Figure 4. Single-stage transonic compressor geometry.

In the single-stage compressor, the rotor contains 16 blades, and the stator has 40 blades. The design mass flow rate was 4.0 kg/s at 37,500 rpm. The total pressure and temperature at the inlet were 101 KPa and 288 K, respectively. The rotor hub section operated at a relative Mach number about 0.9, while the tip section was at about 1.4. The geometry of this single-stage compressor was shown in Figure 4, which is a screen shot from Concepts

NREC's axial blading design software AXCADTM⁴. In this figure, the 3D graphics showed the machine geometry, while the 2D window showed the gas path and the rotor blade shapes. Both the rotor and stator blades are designed by using DCA blades.

To begin with, we calculated the rotor tip section. The rotor tip section was made of a DCA blade, with an inlet blade angle of 60°, exit angle of 53°. The axial chord length was about 2.5 cm, while the maximum thickness to chord ratio was 2%.

To model the blade-to-blade flow field correctly, we need to include streamtube thickness effects in the code. In other words, it is a quasi-three-dimensional problem. The computational domain in the hub to tip direction is of one cell thin, and with radius and curvature effects included in the cell volume calculations. By using the two-dimensional CE/SE solver, the streamtube thickness effects is missing, hence, the rotation source terms can not be balanced out through pressure rise alone in the control volume. The only way to overcome this problem is to develop a three-dimensional CE/SE code for turbomachinery. The blade-to-blade flow then becomes a special case of the general 3D CE/SE solver, with the distance in the hub to tip direction being trimmed down to one cell thin.

In order to address the turbulent shock wave-boundary layer interactions, we also implemented the standard algebraic Baldwin-Lomax turbulence model (with inner-outer layer matching to calculate eddy viscosity) to better assess the loss mechanism associated with the blade row and to compare with the solution obtained from the traditional RK code.

To evaluate that the Euler part of the CE/SE scheme is functioning correctly, we performed calculation using the tip section of the single-stage compressor rotor. To begin with, we chose a relatively coarse grid size of 71 x 41 in the streamwise direction and the blade-to-blade direction, respectively.

Figures 5a and 5b showed the relative Mach number contours obtained from the RK code and the Euler CE/SE code. The freestream Mach number is close to 1.5, which was very close to the test data at 1.45. As can be seen in these two figures, the leading shock from the RK results indicated a more spread-out resolution, while the CE/SE results showed a crisp and tight resolution across the shock. The CE/SE results converged to a nearly steady-state solution, with very minor oscillations in the downstream blade wake region. In contrast to the shock oscillation generated by 2D CE/SE code shown in the previous paragraphs, the location and the strength of the shock remained very steady from the 3D CE/SE code

⁴ AXCADTM is a trademark of Concepts ETI, Inc.

prediction – an anticipated result with the inclusion of the streamtube thickness effects. The comparisons between the traditional CFD method used in RK code and the CE/SE code also showed the high fidelity solution capability of CE/SE algorithm.

For designing highly loaded transonic compressors, the high accuracy prediction capability for shock wave is highly desirable. Upon completion, the CE/SE code can provide a step increase in predicting turbomachinery flow field as well as performances. To examine how the shock was resolved by CE/SE, Figure 5c shows a close-up view with the computational grid superimposed on top of the relative Mach number contours obtained from CE/SE. We can see the width of shock wave was being resolved to about one cell thin, a tremendous improvements over traditional CFD techniques, which at least requires several cells to resolve the shock wave.

There is another interesting phenomenon associated with the computed results, from both the RK and CE/SE. We can clearly see that the shock wave started to smear out a little bit after it entered the blade row. The shock strength after blade LE is somehow weakened, which was predicted by both codes. This might be a result of the curvature effects on the suction surface of the blade, which caused the flow to accelerate and to lose a lot of energy prior to the shock. After consulting with Mr. Tsukasa Yoshinaka, who designed this particular compressor during his tenure at Pratt & Whitney Canada, we are still not sure about the reason, that caused the shock smearing effect inside the blade passage.

Figures 6a and 6b show the predicted static pressure contours from the RK code and the CE/SE code. Similar to the relative Mach number contours, the RK results show a more smeared LE shock wave, especially near the suction side of the blade surface, while the CE/SE scheme resolves shock wave to one cell thin. The peak pressure appeared near the LE of the blade, which was predicted at about 160 KPa by the RK code, 170 KPa by the CE/SE code. The lowest static pressure, which occurred along the first 1/3 chord of the suction surface, showed the flow was being accelerated near this region, which was predicted by both methods. The blade-to-blade loading pattern, with high pressure at the pressure surface of the blade, than the suction surface at the same axial location, was predicted by both codes. The exit static pressure was about 130 Kpa, although predicted by both codes, however, the CE/SE results showed a more smooth solution near the blade trailing edge. Keep in mind that the RK code was a well-established turbomachinery CFD code, written specifically for turbomachinery flows. It has been calibrated over the years for all types of turbomachinery flows. For the CE/SE scheme to be developed to work on rotating machinery, then to predict

blade-to-blade flow results at a level which were comparable or better than the RK results, was a true accomplishment.

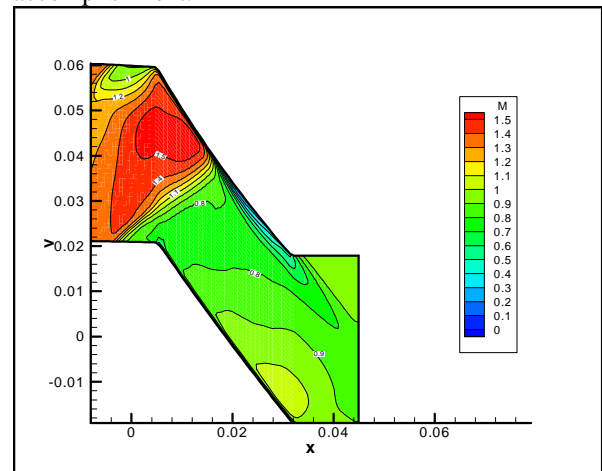


Figure 5a. Relative Mach number contours predicted by the RK code.

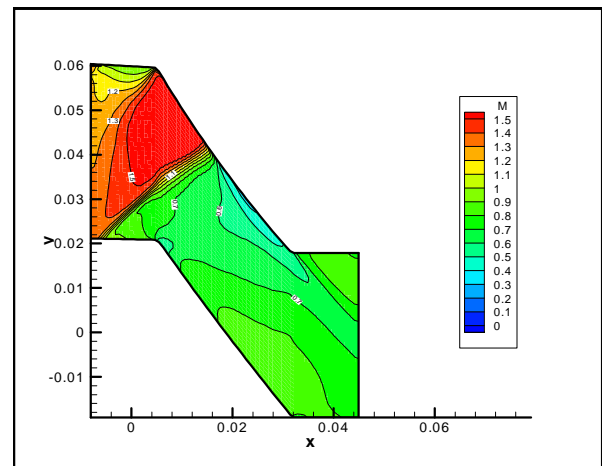


Figure 5b. Relative Mach number contours predicted by the CE/SE code.

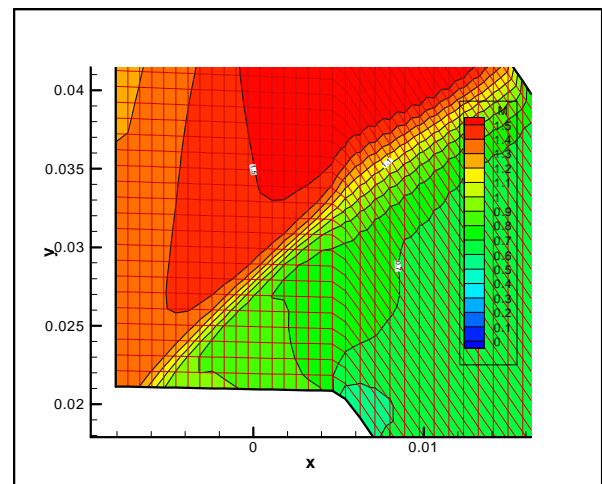


Figure 5c. Close-up view of relative Mach number contours near the leading edge, CE/SE results.

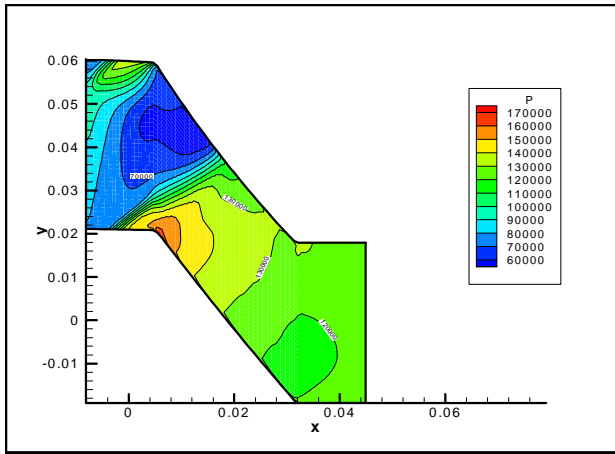


Figure 6a. Static pressure contours predicted by the RK code.

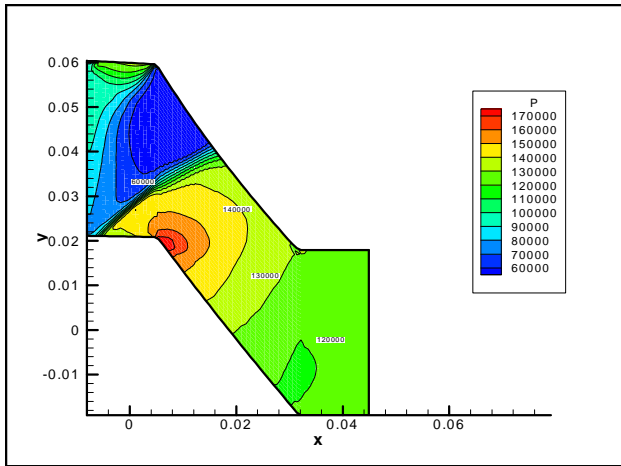


Figure 6b. Static pressure contours predicted by the CE/SE code.

After evaluating the Euler solution, we then proceeded to evaluate the Navier-Stokes solution, with the effects of turbulence included in the computations. For the rest of the test cases calculated, we will only include the Navier-Stokes results, since it represents the flow physics. We use the same blade tip section to begin the evaluation. The grid size has been increased to 201×101 in the axial and blade-to-blade directions, respectively, to

provide resolution near the blade surfaces for possible shock wave-turbulent boundary interaction computations. The grid size remained constant throughout the computation, there was no grid-adaptation method being employed to favor one solver over another in this investigation. The LE blade angle is 60° measured from meridional, while the TE blade angle is 53° .

Figures 7a and 7b showed the computed relative Mach number contours obtained from the RK code and the CE/SE code. In Figure 7a, the RK results showed a detached shock wave near the LE, and the shock wave beginning to spread out close to the suction surface of the blade. This is the location where the shock wave impinging and interacting with the boundary layer near the blade suction surface. The RK results showed a minor growth of the boundary layer caused by the shock wave and there was no shock wave induced separation observed. The boundary layer by the suction surface remained thin throughout the blade surface. The size of the turbulent wake is small and being mixed out quickly by the core flow. In Figure 7b, the CE/SE solution shows a detached LE shock wave, which was computed at the same level of resolution before it split up into a classical λ wave, due to the interaction with the boundary layer. The two branches of the λ wave were clearly observed. This also explains the very widely spread-out solution predicted by the RK code, because it failed to resolve the λ wave on the present grid system. The shock wave induced separation, which was clearly observed at the foot of the λ wave, impacts the downstream wake to extend further into the mixing region. In a highly loaded axial compressor, this phenomenon is usually observed because it causes the subsequent rotor-stator interaction due the non-uniformity of the rotor TE wake in a multiple blade row axial turbomachinery environment. The CE/SE solution shows a very detailed local flow field surrounding the LE, while the RK results suggest the presence of the LE was not being resolved well.

If we put Figure 7a and 7b together, we can see the location of the oblique shock wave predicted by the two solvers is different. The oblique shock wave is pushed further away from the LE as predicted by the RK code, while the oblique shock wave is much closer to the LE as indicated by the CE/SE results. Both computations were based on the same exit static pressure at 125 KPa. The reason for the farther shock location from LE in the RK result is because of the under-resolved shock wave induced separation to lead to a smaller loss associated with the computation. Both solvers predicted, very accurately, the maximum relative Mach number at about 1.4, at a location upstream of the oblique shock wave, prior to the LE. In addition, the passage shock wave was also clearly predicted by both solvers.

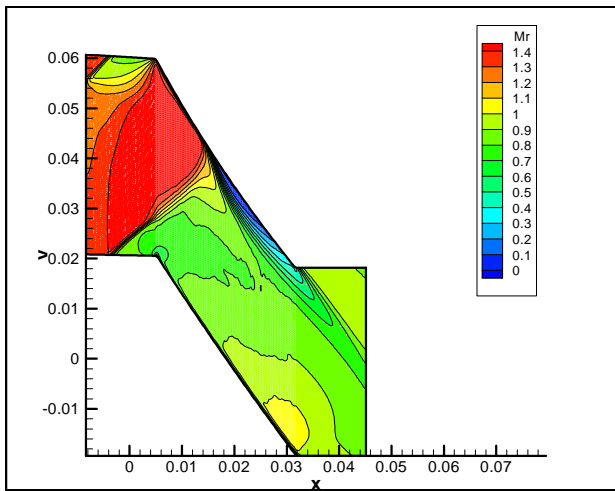


Figure 7a. Relative Mach number contours predicted by the RK code, NS solution.

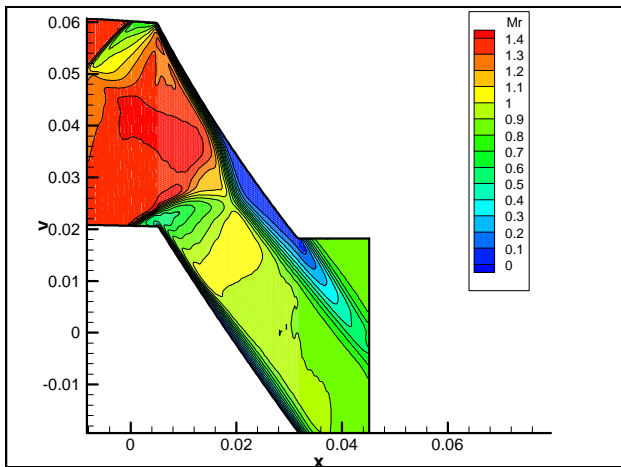


Figure 7b. Relative Mach number contours predicted by the CE/SE code, NS solution.

NASA Rotor 37

The second test case that we selected was the legendary NASA rotor 37. This was a research program for axial flow compressors being conducted at NASA Glenn Research Center about 20 years ago. There were four rotors being studied in this research, namely rotor 35, 36, 37, and 38. Rotors 37 and 38 represented a pressure ratio about 2.05, while rotors 35 and 36 generated a pressure ratio close to 1.85. Each compressor stage contained a rotor and a stator. Measurement data were taken downstream of the stator to address the pressure ratio, efficiency, and flow angle at different design speeds. There were no data taken at the rotor exit, prior to the stator LE because the spacing between the blade row was too narrow to allow proper instrumentations and data samplings. All four stages were designed for a mass flow of 20.0 kg/s and a rotor tip speed of 455 m/s. The radial distributions of rotor inlet meridional velocity are almost

the same for all four rotor geometry, with a peak value of about 215 m/s at the mean section, and a minimum value of 185 m/s at both hub and tip locations.

The test data for Rotor 37 was later used as a blind test case for CFD code validations. Turbomachinery investigators worldwide were invited to submit their computational results based on the published geometry and test conditions before the test results were revealed. Once the test data were compared to all the CFD results submitted and released to the public, CFD researchers were surprised by the discrepancies between the test data the computational results. The CFD results spread over a wide range in terms of pressure ratio, stage efficiency, and pitched averaged radial flow profiles. The comparisons with the test data turned out to be rather disappointing. The advancements in CFD technology over the past twenty years have been significant enough to make CFD a practical tool for turbomachinery designs. However, rotor 37 test data still presents a challenge for most of the CFD code to predict close matches for the radial flow profiles. Based on the interesting story and its rich history in the making, we selected rotor 37 as one of the test cases to verify the prediction capability of CE/SE. Although the blade-to-blade flow field in the present Phase I project was not appropriate to be compared with the full three-dimensional test data, the intriguing history and the challenging supersonic rotor flow field has provided enough reason to look into the heart of rotor 37. In possible Phase II project, full three-dimensional calculations of Rotor 37 using the traditional CFD technique and the CE/SE scheme definitely presents the best opportunity to address the advantages and/or shortcomings of the CE/SE scheme when compared to the traditional CFD methods.

The geometry of the Rotor 37 was shown in Figure 8. In this figure, the 3D graphics showed the machine geometry, while the 2D window showed the gas path and the rotor blade shapes. The rotor was composed of 36 blades, while the stator had 46 blades. At the design point, the rotational speed was 17,200 rpm. The inlet total pressure and total temperature were 101.3 KPa and 288 K. The design relative Mach number was about 1.3 at the hub, then increased to about 1.5 level for the mean section, then to 1.8 near the blade tip section.

We first looked at the rotor hub blade cross-section. The hub blade shape was designed using the MCA blade family. The inlet blade angle was 50°, while the exit blade angle was 23° to provide a turning of 27°. The axial chord length was 4.3 cm, and the tangential chord length was 3.5 cm. The maximum thick to chord ratio was 8%.

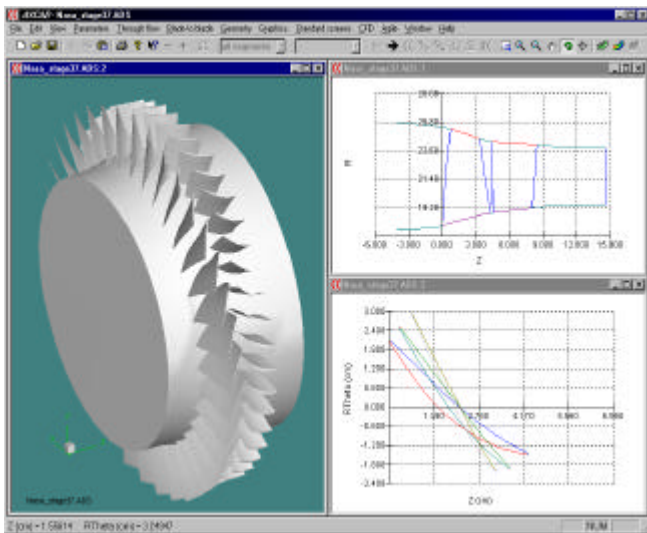


Figure 8. The full stage geometry, meridional flow path, and the rotor blade hub, mean, and tip cross-sections of the legendary NASA Rotor 37.

We used a computational grid size of 201×101 in the axial and the blade-to-blade directions, respectively, to conduct full Navier-Stokes calculation for both the RK code and the CE/SE code. Once again, the geometry and boundary condition inputs were identical for both solvers. The computational mesh remained the same throughout the numerical simulation, there was no grid adaptation technique employed in either of the two solvers to bias the computational results.

The relative Mach number contour for the hub blade cross-section was plotted in Figures 9a and 9b by using the RK code and CE/SE code, respectively. The maximum relative Mach number about 1.2 was clearly captured in front of the shock wave in both cases. The CE/SE code, however, indicated a sharper shock wave and thicker boundary layer. The strength and location of the shock were a bit different, too. Recall that both the RK and the CE/SE codes predicted nearly the same inviscid flow physics, as shown in Figure 5. Therefore, the discrepancies in shock strength and location were mainly due to the presence of a boundary layer. The presence of a boundary layer on the blade suction surface resulted in an altered boundary condition for the shock wave. These interactions are nonlinear phenomenon and, thus, were not likely to be predicted with a simplified boundary layer theory. The question now is which method predicted a more realistic boundary layer thickness. Unfortunately, we did not have test data to justify this issue. Nevertheless, we know that the shock wave will likely induce flow separations and sudden boundary layer growth due to the pressure jump across a shock wave. The CE/SE results seemed to better justify the flow physics. The passage shock, which strength is weak in nature, was merely captured by the RK code, as seen in Figure 9a, and the results suggested the RK would not be able to resolve the passage shock if the grid density

is lower than the current one. On the other hand, the CE/SE code showed a distinctive resolution of the passage shock and more detail flow gradients across the passage shock wave. This was shown in Figure 9b. The wake region was captured well by both codes, and the CE/SE method showed an unsteady wake pattern coming off the blade TE.

The other interesting observation can be seen from the loading predictions of these two codes. The RK code showed the flow accelerated for most of the blade passage. For about 80% of the chord length, the flow was experiencing acceleration. Because of this acceleration, the flow speed, once again, stayed at or above sonic speed for approximately 80% of the blade passage. This indicated the RK code predicted the hub section was operating at its choke condition. If this happened, the rotor would not be able to add work efficiently to the fluid to provide the necessary pressure rise. The test data, however, showed the rotor was operating at a very high performance level with a measured stage efficiency at nearly 88%. This represented a condition, which for a choked rotor, could not possibly be achieved. The CE/SE results also showed slight flow acceleration downstream of the shock wave, then the flow started to diffuse, to slow down to a relative Mach number of 0.8 at the blade TE.

After finishing the investigation for the hub section of Rotor 37, we proceeded to study the blade-to-blade flow field of the rotor mean blade section. The mean section was designed by using the MCA blade family. The axial chord length was 3.4 cm and the tangential chord length was 4.4 cm. The inlet blade angle was 54° , while the exit blade angle was 47° . The maximum thickness to chord ratio was about 5.2%. The geometry of the mean blade section was shown in Figure 3.18.

The computational grid size was 201×102 in the axial and blade-to-blade directions, respectively, and the grid size and number remained constant throughout the computations. At the mean section, the computed relative Mach number contours were shown in Figures 10a and 10b, obtained from the RK and the CE/SE methods. First of all, similar to other supersonic blade sections studied, the CE/SE code showed excellent resolution of the passage shock wave, as shown in Figure 10b. Although in Figure 10a, the RK code also predicted the presence of the passage shock, the RK results showed a very washed out compression wave with minor flow gradient across it. The designed maximum relative Mach number was around 1.5. This was computed accurately by both codes. Other than the maximum relative Mach number, the rest of the blade-to-blade flow results showed significant difference between the two codes.

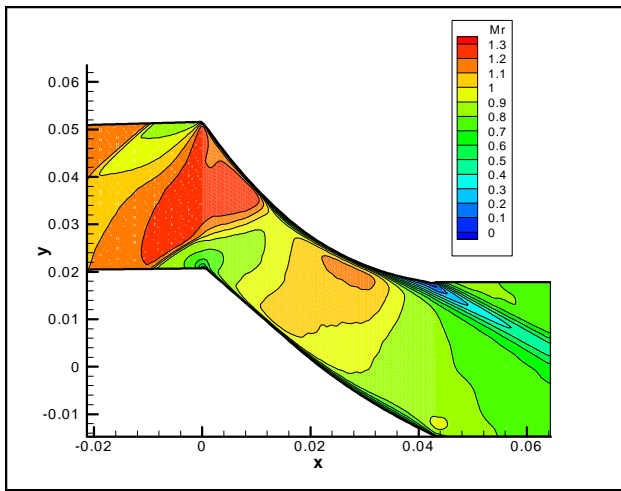


Figure 9a. Relative Mach number contours predicted by the RK code, NS solution.

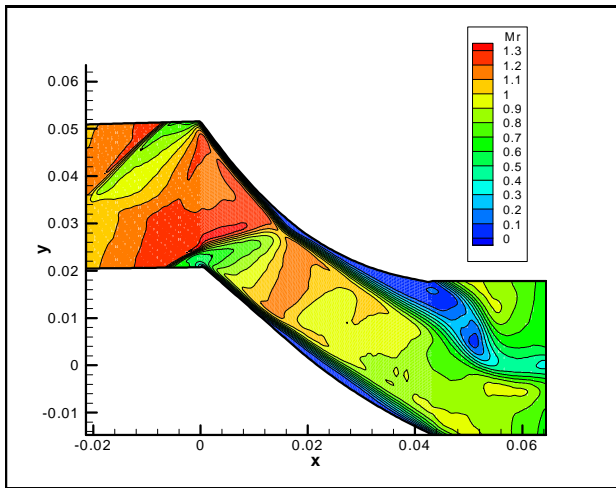


Figure 9b. Relative Mach number contours predicted by the CE/SE code, NS solution.

First, the RK code, similar to the hub section, predicted the mean section was also operating at choke condition. The flow accelerated throughout the entire blade-to-blade passage, from LE to TE, then formed a shock wave at the TE. The flow speed reduced to subsonic and the pressure rose outside the blade passage. This was similar to what was observed in RK results for the hub blade section. As stated earlier, Rotor 37 had a high performance curve, with peak stage efficiency at 88%. For the mean section to be operating at choke condition was not likely to happen based on the test data. On the contrary, the CE/SE predicted a very reasonable blade-to-blade loading pattern, with an oblique shock wave in front of the LE, then the flow speed was reduced to subsonic, gradually, to a relative Mach number of 0.8 at the blade exit. This was consistent with the test result. In addition to the loading pattern prediction, the CE/SE code also predicted a shock induced separation at the blade suction surface, and a nicely resolved wake region. Because of the shock induced separation and the thicker

boundary layer calculated by the CE/SE code, the solution predicted a larger loss system compared to the RK results.

To investigate why the RK code would predict a choked condition for both the hub and mean section, we performed an additional test to better understand the mechanism. We started to increase the exit static pressure, which was fixed as the downstream boundary condition at the end of the computational domain, to 5%, 10%, even to 20% higher than its original value, to see if the shock wave structure changed or not. To our surprise, the RK code still predicted a choked flow condition for the mean section, under a circumstance which the exit pressure was raised 20% higher than the original value. Under such a high-pressure situation, the shock wave was not pushed out of the LE, but instead, it only moved slightly upstream of the original position, as shown in Figure 10a. The reason remained unclear as to why the RK prediction was unrealistic.

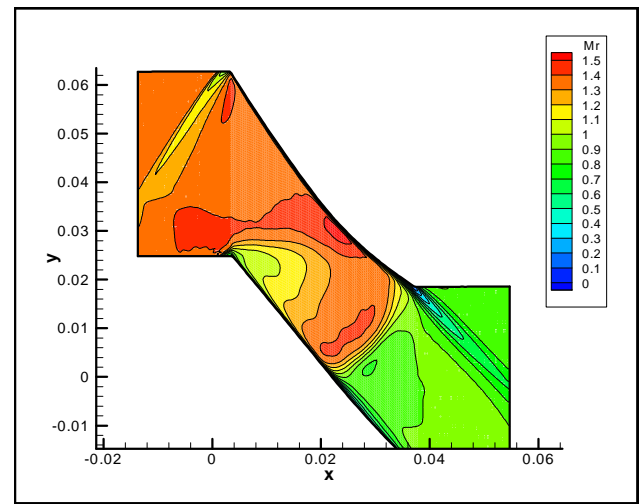


Figure 10a. Relative Mach number contours predicted by the RK code, NS solution.

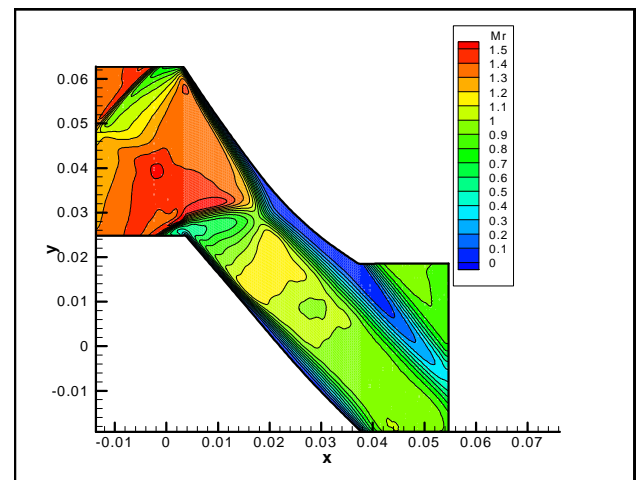


Figure 10b. Relative Mach number contours predicted by the CE/SE code, NS solution.

Finally, we moved to examine the tip section of Rotor 37. Once again, the tip section was designed by using the MCA blade family. The axial chord length was 2.6 cm and the tangential chord length was 4.9 cm. The inlet blade angle was 64° , while the exit blade angle was 53° , providing 11° of turning. The maximum thickness to chord ratio was about 3.0%.

For Navier-Stokes calculations of the tip section, we again chose a grid size of 201×101 in the axial and the blade-to-blade directions. Figures 11a and 11b showed the computed relative Mach number contours from the RK and the CE/SE code. The designed maximum relative Mach number at the tip section was close to 1.7, a relative high Mach number for supersonic blade sections. This was a result of the increasing radius toward the tip section while the machine is moving at a constant speed. The RK results, shown in Figure 11a, indicated the LE oblique shock wave impinging almost at the TE of the blade suction surface, then bounced off the wall, to form a nearly normal shock and terminated at a location at about 50% on the pressure surface. There was a small shock induced separation region near the TE of the blade suction surface observed. The computational mesh was not sufficient to resolve the further reflection or the ‘shock chain’ pattern for the RK code. The wake region was clearly larger compared to the ones predicted by the RK code in the hub and mean sections, probably because of the induced separation in front of the wake. The passage shock wave was almost not being resolved, there only existed a very small gradient to indicate a compression wave, as predicted by the RK code.

In Figure 11b, the CE/SE code showed an extremely interesting result. The shock wave pattern, in general, was similar to what was computed by the RK code. However, the CE/SE code solution showed finer resolution of the complex shock structure and flow pattern. In this figure, the attached LE oblique was formed and started to interact with the suction surface boundary layer at a location close to the TE. The boundary layer immediately grew thicker and an obvious induced separation was observed. This agreed with what was calculated by the RK code, only the resolution of the shock wave was better. Then the shock wave was reflected off the suction surface boundary layer, across the blade passage, to impinge upon at about half way on the pressure surface. This reflected shock wave then interacted with the pressure surface boundary layer to cause the boundary layer to grow thicker in the neighborhood of the interaction point. Then the shock wave, already being reflected once from the suction surface, being bounced off the pressure surface again, to out of the blade passage to interact with the wake coming off the suction surface. The second reflection was completely unseen in the RK results. This shock sequence formed a shock chain throughout the blade passage and in the wake region. The blade wake, hence, grew into a

highly unsteady state, formed a wavy wake pattern downstream of the blade passage. The CE/SE computation has been carried on long enough in the time domain to confirm the unsteady nature of the turbulent wake, due to its interactions with the shock chain. In the CE/SE results, the shock chain pattern was clearly resolved. This indicated that in the CE/SE code, the numerical dissipation effect was at a minimum level to preserve the reflected shock strength. On the contrary, the numerical dissipation in the traditional central-differencing scheme used in the RK code was not able to preserve the reflected strength to resolve the shock chain. This also explained why the very weak passage shock was still captured beautifully by the CE/SE method, yet not by the RK code.

Throughout the study of Rotor 37’s hub, mean and tip blade sections, we can conclude that the CE/SE produced much detail and accurate computational results compared to the traditional RK turbomachinery CFD code, by using the same computational grid and machine operating conditions.

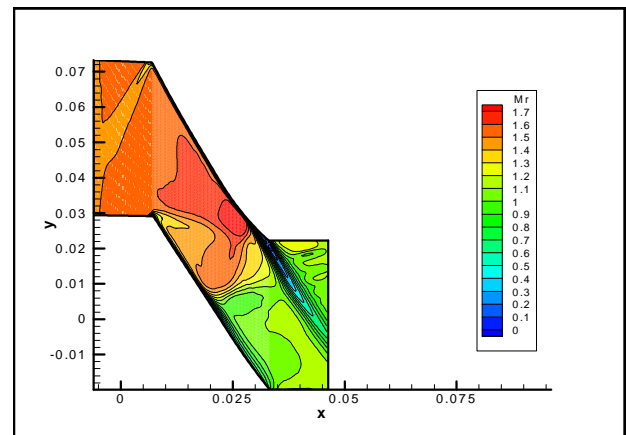


Figure 11a. Relative Mach number contours predicted by the RK code, NS solution.

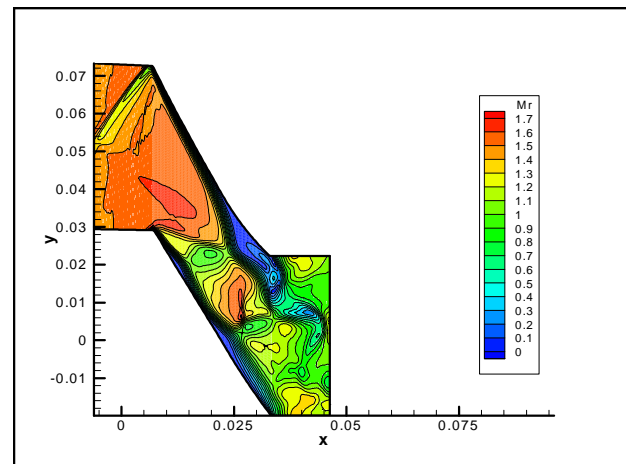


Figure 11b. Relative Mach number contours predicted by the CE/SE code, NS solution.

High Pressure Ratio Turbine

Two previous test cases were axial compressors. To demonstrate the validity of the developed CE/SE method is suitable for all turbomachines, we chose a single-stage high pressure ratio turbine as a test case. The geometry and aerodynamic data was taken from the paper entitled “The Design, Performance and Analysis of a High Work Capacity Transonic Turbine,” co-authored by Bryce, J. D., Litchfield, M. R., and Leversuch, N. P., published in the October, 1985 issue of Journal of Engineering of Gas Turbine and Power, ASME.

The stator blade row is composed of 40 vanes. Each blade is made of large leading edge radius for the purpose of circulating cooling fluid inside the blade to accommodate the incoming high temperature combustion gas. Only the hub cross-section contour of the blade was given in the paper while leading edge and trailing edge blade angles were missing. Because of the very large leading edge radius, the stator blade cross-sections look like a “Tear Drop.” The rotor blade row is composed of 89 blades. The designed pressure ratio through the single-stage turbine was 4.48. The geometry, flow path, stator blade cross-sections, and the rotor blade cross-section of the single-stage high pressure ratio turbine was shown in Figure 12.

The inflow conditions were given in terms of performance parameters (pressure, work capacity, aerodynamic loading, and mean blade speed function, etc.). Therefore, we have to transform these parameters into standard testing conditions (absolute pressure and temperature, mass flow rate, flow swirl angle, and rotational speed). The gas path was deduced from a plot shown in the reference. Measurement data of the stator mean section was presented in terms of Mach number in the paper. The measured absolute Mach number at the exit of the stator mean section was 1.295. In this particular design, in which the design pressure ratio was 4.48 (total-to-total), the measured flow in the rotor blade was near choke, and the exit relative flow is close to sonic. This was a very rare design to have both the stator and the rotor choked.

We began by examining the stator flow field. The stator had a relatively two-dimensional geometry, therefore we chose to analyze the mean section of the ‘tear-drop’ nozzle. The mean section was designed using Pritchard turbine blade family. The inlet blade angle was 50° , and the exit blade angle was 74° . The axial chord was 3.6 cm, while the tangential chord was 7.1 cm. The large LE radius was 7 mm, and TE radius was 0.6 mm. The throat was about 1.1 cm.

The computation mesh used for this calculation was 71×41 . The computed Mach number contours were shown in Figure 13a and 13b for the RK and the CE/SE

code results. The inlet Mach number was about 0.1, as shown by both codes. Both codes predicted the exit Mach number to be 1.3, which was in excellent agreement with the test data of 1.295. This turbine stator provided a large amount of acceleration, and the was the reason why the LE was shaped like a tear-drop, in order to provide more contraction effects for flow acceleration. The RK results only captured a minor wake region generated by the TE, as shown in Figure 13a. The CE/SE code, showed an excellent wake formation and mixing with the core flow, can be seen in Figure 13b. Nevertheless, the CE/SE code predicted the Mach number contours were almost normal to the flow path while the RK code showed the contour lines tilted toward one surface after the flow turning supersonic. The CE/SE code also predicted a thicker boundary layer for this particular blade section.

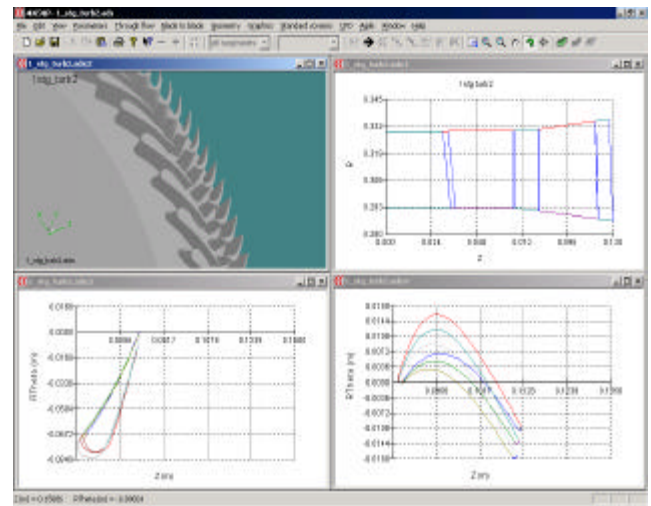


Figure 12. The geometry, gas path, stator blade cross-sections, and the rotor blade cross-sections of the single-stage high pressure ratio turbine.

Next, we studied the rotor mean section of this single-stage high pressure ratio turbine. The rotor blade mean section was designed by using the Pritchard turbine blade family. The inlet blade angle was 60° , while the exit angle was -58° , providing a turning of 118° . The axial chord length was 3.0 cm, while the tangential chord length was 0.15 cm. Both the LE and TE radius were on the order of 0.5 mm. The throat was 1.0 cm.

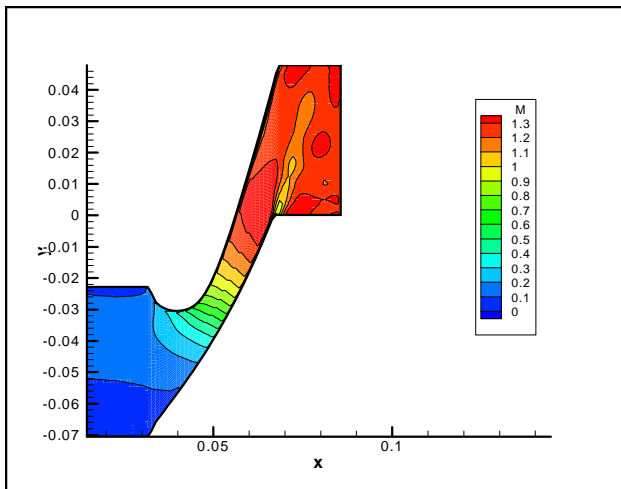


Figure 13a. Mach number contours predicted by the RK code, NS solution.

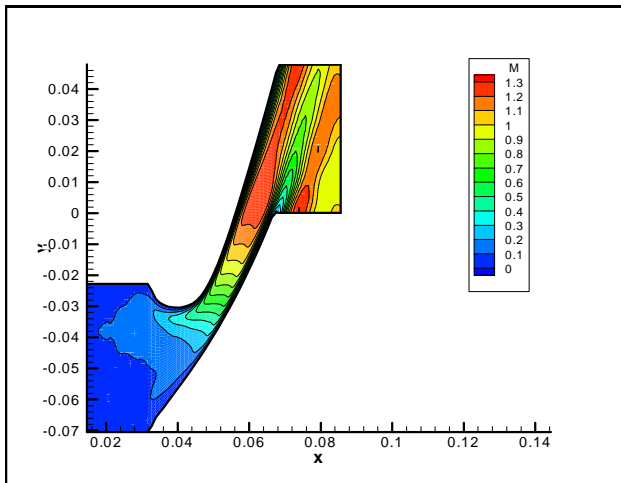


Figure 13b. Mach number contours predicted by the CE/SE code, NS solution.

We used a computational grid of 71 x 41 in the axial and blade-to-blade directions for this mean blade section calculations. Figure 14a and 14b showed the computed relative Mach number contours obtained from the RK code and the CE/SE code. As stated earlier in the description of this high pressure ratio turbine, the measured exit flow of the rotor was near sonic, close to choke condition. In Figure 14a, the RK code predicted an exit relative Mach number of 0.6 to 0.7, a level much too low compared to the test data. There was also a weak momentum layer near the suction surface of the blade, due to the incidence at the inlet caused by the thicker turbine blade near the LE. In Figure 14b, the CE/SE code predicted an exit Mach number about 0.95, at a level much closer to the test data compared to the RK results. In addition, the majority of the blade passage flow at the exit plane was uniformly composed of Mach 0.95 flow. On the other hand, the RK results showed a more distributed exit Mach number.

For this single-stage high pressure ratio turbine case, the CE/SE results compared very well with the test data for both the stator and rotor calculations. The RK results showed a reasonably good agreement with data for the stator blade mean section, however, the rotor results were off by at least 30% compared to data. This study has again indicated the CE/SE code not only can resolve detail local flow field better than the traditional RK turbomachinery CFD code, but also can provide highly accurate computational results when compared with test data. For this reason, the future development for the CE/SE code applied to turbomachinery flow field analysis to improve turbomachinery design capability is definitely needed and highly valuable.

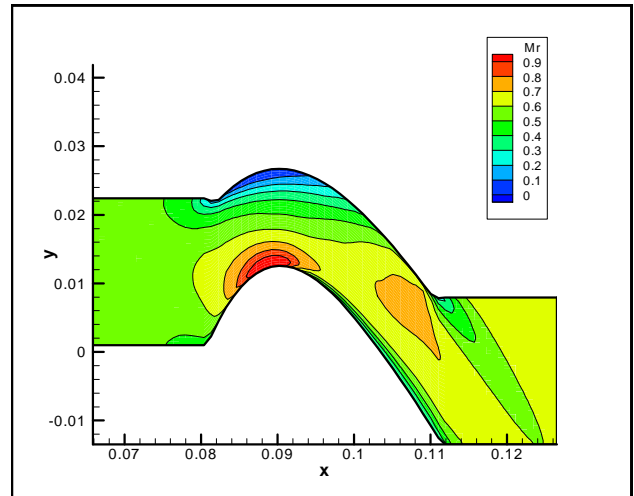


Figure 14a. Relative Mach number contours predicted by the RK code, NS solution.

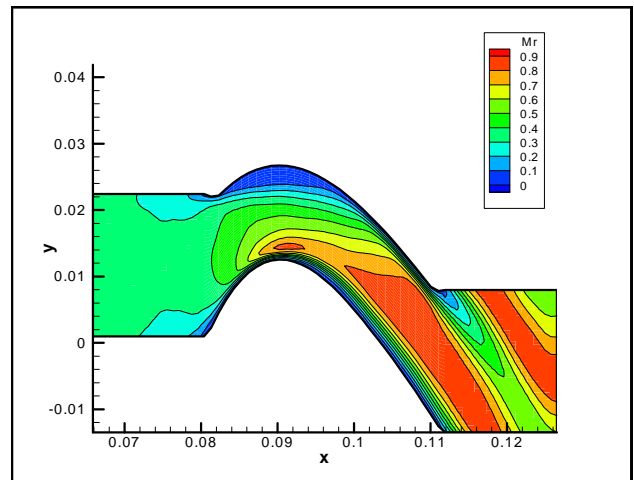


Figure 14b. Relative Mach number contours predicted by the CE/SE code, NS solution.

SUMMARY

The present research emphasized the development and validation for the space-time CE/SE method for rotating machinery to complement an existing turbomachinery CFD code, in order to provide better predictions for turbomachinery flows. The CE/SE method has demonstrated the potential to replace the widely used, explicit Runge-Kutta algorithm in the turbomachinery CFD industry to provide more accurate and reliable results. It is expected that the CE/SE method will be applied to rotor-stator interaction and a wide range of turbomachinery related flow fields when the development and validation processes are completed under research efforts.

In summary, the accomplishments of the present research are as follows.

- The three-dimensional space-time CE/SE code for rotating machinery has been developed for the first time, with emphasis on the effects of adverse pressure gradient, rotational flow predictions for turbomachinery flows.
- Algebraic Baldwin-Lomax turbulence model has been implemented into the developed CE/SE code to provide loss prediction mechanism for turbomachinery flow calculations. This is the first time for a traditional turbulence model to be integrated with the CE/SE method.
- Fundamental validation studies have been performed to provide understanding of the prediction capability of the CE/SE method for rotating machinery for both Euler and Navier-Stokes solutions.
- The CE/SE code was used to calculate a single-stage compressor rotor blade sections. The computational results have been compared with the RK code results.
- The CE/SE code was validated to calculate the NASA Rotor 37 blade sections. Results have been compared with the RK results and summarized.
- The CE/SE code was tested for a single-stage high pressure ratio turbine for both the stator and rotor blade sections. The CE/SE results showed excellent agreement with test data and superceded the computed results by the RK code.

ACKNOWLEDGMENT

The research was funded by the NASA Glenn Research Center under Contract No. NAS3-00005. The financial support is highly acknowledged.

REFERENCES

1. Sharma, O.P, Ni, R.H. and Tanrikut, S., "Unsteady Flows in Turbines – Impact on Design Procedure", AGARD Lecture Series 195, "Turbomachinery Design Using CFD", May, 1994.
2. Chang, S.-C., "The Method of Space-Time Conservation Element and Solution Element – A New Approach for Solving the Navier Stokes and Euler Equations", J. of Comp. Phys., Vol. 119, pp. 295-324, 1995.
3. Chang, S.-C., Yu, S.-T., Himansu, A., Wang, X.-Y., Chow, C.-Y., and Loh, C.-Y., "The Method of Space-Time Conservation Element and Solution element – A New Paradigm for Numerical solution and Conversation Laws", Computational Fluid Dynamics Review 1997, John Wiley and Sons, UK.
4. Chang, S.-C., Wang, X.-Y., and Chow, C.Y., "The Method of Space-Time Conservation Element and Solution element – Applications to One-Dimensional and Two-Dimensional time-Marching Flow Problems", AIAA 95-1754, 12th AIAA CFD Conference, San Diego, CA, 1995.
5. Wang, X.-Y., Chow, C.Y., and Chang, S.-C., "An Euler Solver Based on the Method of Space-Time Conservation Element and Solution Element", Proceeding of the 15th Int. Conf. Num. Methods Fluid Dynamics, Monterey, CA, 1996.
6. Dawes, W. N., "A Computer Program for the Analysis of Three-Dimensional Viscous Compressible Flow in Turbomachinery Blade Rows," Whittle Laboratory, Cambridge, UK, 1988.
7. Dawes, W. N., "The Development of a Solution Adaptive 3D Navier-Stokes Solver for Turbomachinery," AIAA 91-2469, 1991.
8. Adamczyk, J.J., "Model Equation for Simulating Flows in Multistage Turbomachinery", ASME 85-GT-226, 1985.
9. Adamczyk, J.J., Celestina, M.L., Beach, T.A., and Barnett, M., "Simulation of Three-Dimensional Viscous Flow within a Multistage Turbine", ASME J. of Turbomachinery, Vol. 112, pp. 370, 1990.
10. Rhie, C.M., Gleixner, A.J., Spear, D.A., Fischberg, C.J., and Zacharias, R.M., "Development and Application of a Multistage Navier-Stokes Solver – Part I : Multistage Modeling Using Bodyforces and Deterministic Stresses", ASME 95-GT-342, 1995.
11. Hall, E.J., "Aerodynamic Modeling of Multistage Compressor Flow fields – Part 2 : Modeling Deterministic Stresses", ASME 97-GT-345, 1997.
12. Rai, M.M., "Navier-Stokes Simulation of Rotor/Stator Interaction Using Patched and Overlaid Grids", J. of Propulsion and Power, Vol. 3, pp. 387, 1987.

13. Jorgenson, P.C.E., Chima, R.V., "An Explicit Runge-Kutta Method for Unsteady Rotor/Stator Interaction", AIAA 88-0049, AIAA 26th Aerospace Science Meeting, Reno, NV, 1988.
14. Fan, S., and Lakshminarayana, B., "Time-Accurate Euler Simulation of Interaction of Nozzle Wake and Secondary Flow with Rotor Blade in an Axial Turbine Stage Using Nonreflecting Boundary Conditions", AEME J. of Turbomachinery, Vol.118, pp. 663, 1996.
15. Hah, C., Puterbaugh, S.L., and Copenhaver, W.W., "Unsteady Aerodynamic Flow Phenomena in a Transonic Compressor Stage, J. of Propulsion and Power, Vol. 13, No. 3, 1997.
16. Nozaki, O., Kikuchi, K., Nishizawa, T., Matsuo, Y., Hirai, K., and Kodama, H., "Three-Dimensional Viscous Analysis of Rotor-Stator Interaction", AIAA 99-0239, 37th AIAA Aerospace Science Meeting and Exhibit, Reno, NV, 1999.
17. Lakshminarayana, B., "An Assessment of Computational Fluid Dynamic Technique in the Analysis and Design of Turbomachinery – The 1990 Freeman Scholar Lecture", J. of Fluids Engineering, vol. 113, pp.315, 1991.
18. Jameson, A., Schmidt, W., and Turkel, E., "Numerical Simulation of the Euler Equations by Finite Volume Methods of Using Runge-Kutta Time Stepping Schemes", AIAA 81-1259, 1981.
19. Harten, A., "High Resolution Schemes for Hyperbolic Conservation Laws", J. Computational Physics, Vol. 49, pp. 357-393, 1983.
20. Cook, G., "High Accuracy Capture of Curved Shock Fronts Using the Method of Space-Time Conservation Element and Solution Element", AIAA 99-1008, 37th AIAA Aerospace Science Meeting and Exhibit, Reno, NV, 1999.
21. Yoshinaka, T. and LeBlanc, A. D., "Test Results from an Analytically Designed Axial Compressor Stage of 1.65 : 1 Pressure Ratio", SAE Paper No. 800629, 1981.
22. Leach, K, Thulin, R. and Howe, D., "Turbine Intermediate Case and Low-Pressure Turbine Component Test Hardware Detailed Design Report", NASA CR-167973, January, 1982.
23. Chima, R.V., "Calculation of Tip Clearance Effects in a Transonic Compressor Rotor", ASME J. of Turbomachinery, Vol. 120, pp. 131, 1998.